

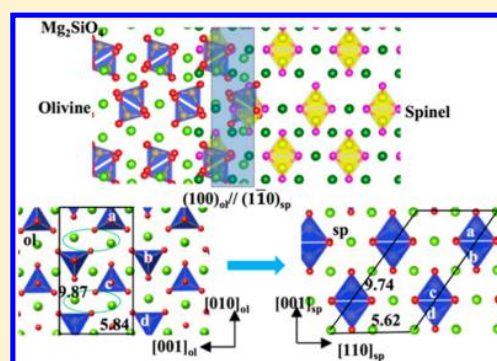
Energy Landscape and Crystal-to-Crystal Transition of Ternary Silicate Mg_2SiO_4

Shu-Hui Guan, Xiao-Jie Zhang, and Zhi-Pan Liu*

Collaborative Innovation Center of Chemistry for Energy Material, Key Laboratory of Computational Physical Science (Ministry of Education), Shanghai Key Laboratory of Molecular Catalysis and Innovative Materials, Department of Chemistry, Fudan University, Shanghai 200433, China

S Supporting Information

ABSTRACT: Solid-to-solid phase transition, although widely encountered in Nature, challenges persistently our current theory for predicting its complex kinetics and rich microstructures in transition. As an important representative for A_2BO_4 oxide, olivine (Mg_2SiO_4) to spinel solid phase transition was hotly debated for its unusual kinetics with complex cation and anion movement. Here we, via novel first-principles based global potential energy surface sampling, resolve the potential energy surface of Mg_2SiO_4 and the lowest energy pathway of the olivine-spinel solid phase transition. Instead of the traditionally regarded mechanism via shearing close-packing oxygen lattice, we identify an unprecedented pathway involving silicate oxoanion (SiO_4^{4-}) rigid-body rotation and translation in the reaction, which may only be expected in molecular crystal transformation. While the anions and cations move synchronously, it is the coordination change of Mg^{2+} in reaction, from octahedral to tetrahedral sites that cause the high barrier. The replacement of Mg cation by Fe and Zn cations is found to substantially reduce the barrier of crystal transformation. Although the reaction do involve significant shearing with a $[001](010)$ slip system, leading to the seemingly early formation of O sublattice, our theoretical results suggest that the phase transition is governed by incoherent nucleation and growth due to the lack of coherent heterophase interfaces. The theoretical results are of general importance for understanding the stability and phase transition mechanism in silicate group materials.



1. INTRODUCTION

Recent years have seen tremendous interests on solid-to-solid phase transitions for their important applications in many fields, for example, chemical synthesis and phase-change materials. Being abundant in Earth's crust and representative for silicate group materials, olivine (mainly Mg_2SiO_4 , Pbnm , #62) will undergo solid phase transition under pressures forming other denser polymorphs, i.e., spinel (ringwoodite, $Fd\bar{3}m$, #227) and modified spinel (wadlysleyite, $Imma$, #74).¹ The solid transformation from olivine to spinel (Figure 1), for its appreciable density change ($\sim 8\%$), is regarded as the cause of deep-focus earthquakes.^{2–5} Despite extensive studies in the past 40 years, the current knowledge on the pathway of the reaction is limited, and the role of shear stress on the transition remains much debated. This dilemma could be largely attributed to the unusual reaction kinetics of Mg_2SiO_4 solid phase transition, where a large volume reduction couples with multiple atom displacement patterns of O anions and two different cations (Mg and Si). The energy profile of such complex solid phase transition reactions is, unlike molecular reactions, extremely challenging to establish for the lack of tools to resolve key intermediate phases and reaction patterns of collective atom displacement.

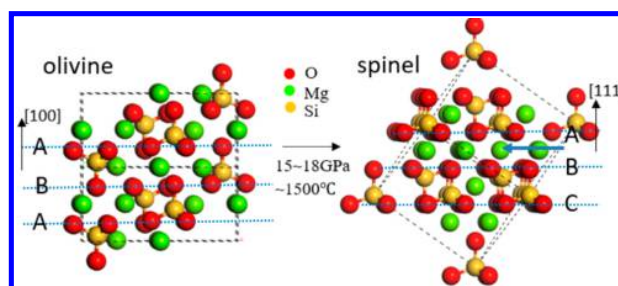


Figure 1. Mg_2SiO_4 structures for olivine (Pbnm) and spinel ($Fd\bar{3}m$) phases. The O sublattice has a hcp (ABAB...) packing in olivine and a fcc (ABCABC...) packing in spinel.

As common in A_2BO_4 oxides, the O sublattices in both olivine and spinel shown in Figure 1 have close-packed structures, hexagonal close-packing (hcp) for olivine and face-centered close-packing (fcc) for spinel. In both oxides, Mg cations occupy the octahedral sites (MgO_6) and Si cations occupy the tetrahedral sites (SiO_4). The major difference

Received: September 5, 2016

Revised: October 11, 2016

Published: October 17, 2016

occurs in the arrangement of Mg and Si cations in between O close-packing layers, where mixed Mg/Si occupancy are present in olivine while a layer of uniform Mg occupancy appears in spinel (indicated by the blue arrow in Figure 1).

By exploiting the structural similarity of O sublattice between olivine and spinel, Poirier⁶ first proposed that the coherent shear of the oxygen sublattice on olivine $(100)_{\text{ol}}$ close-packed plane triggers the olivine-spinel transformation, which is referred as the martensitic type diffusionless phase transition mechanism in early literature.⁶ This mechanism suggests the presence of coherent $(100)_{\text{ol}}//\{111\}_{\text{sp}}$ interfaces and the shear-related coherent growth, but does not answer how cations travel across the close-packing O layers. The orientation relationship (OR) by aligning the close-packing O layer was indeed observed by high-resolution transmission electron microscopy (TEM) studies.^{7–11}

However, new observations were reported in recent years, which question the simple shear mechanism of O close-packing layers. The observed slow kinetics even at high temperatures (1500 °C) implies the involvement of atom diffusion in the transition;⁵ and the critical roles of grain-boundary and dislocations in the phase growth kinetics suggests a fracture-related incoherent nucleation and growth mechanism.^{4,12–14} Furthermore, it was found that the spinel lamellae in the host olivine may in fact not orient uniformly as $(100)_{\text{ol}}//\{111\}_{\text{sp}}$ but can be rather random, which is also against the coherent-interface governed kinetics. To reconcile above, a hybrid mechanism by coupling martensitic and diffusional mechanism, named as pseudomartensitic mechanism, emerges to rationalize the slow kinetics of cations. By finding the early appearance of $(400)_{\text{sp}}$ peaks from in situ X-ray diffraction (XRD), Furnish and Basset¹⁵ and Chen et al.¹⁶ suggested the early formation of O sublattice, that is, the motion of oxygen atoms precedes appreciably the reordering of cations that is a gradual, thermally activated process. The pseudomartensitic mechanism, however, lacks support at the atomic level.

In this work we utilize novel stochastic surface walking (SSW) potential energy surface (PES) global structure search and reaction pathway sampling^{17,18} based on first-principles calculations, to understand the long-standing puzzles on the mechanism and kinetics in Mg_2SiO_4 phase transitions. We explore the PES of Mg_2SiO_4 phases, which discovers large energy gap between crystalline and amorphous phases for this stable silicate system. We reveal the lowest energy pathway of olivine-spinel solid phase transition and found that, surprisingly, the phase transition does not involve the shear of the close-packing O layers but all atoms move synchronously featuring with the rigid-body nature of silicate oxoanion (SiO_4^{4-}). From the mechanism, we conclude that the olivine-spinel transition is short-range reconstructive in nature and cannot be regarded as simple martensitic or pseudomartensitic transition. The origin for the barrier in the solid phase transition is also discussed according to the reconstructive mechanism.

2. METHODS AND CALCULATION DETAILS

2.1. Reaction Pathway Sampling Based on the SSW Method. In this work, the recently developed SSW method is first utilized to explore the PES of the Mg_2SiO_4 phase space, which takes advantage of the global optimization functionality of SSW method (see our previous work for detailed methodology of SSW^{19–21}). The SSW based reaction sampling (SSW-RS) is then utilized to sample the solid reaction pathways, exhaustively and unbiasedly, from which we obtain

the crystal-to-crystal solid phase transition pathway between olivine and spinel.

Here we outline the SSW-RS method briefly. The SSW-RS is based on SSW global optimization method and is targeted for find one-step or short-pathway reactions. The SSW method is able to explore complex PES to identify unexpected new structures and at the mean time to collect the reaction pathways leading to them. For solid phase transitions, this is to identify the one-to-one correspondence for lattice ($L(e_1, e_2, e_3)$, e_i being the lattice vector) and atom (q_i , $i = 1, \dots, 3N$, N is the number of atoms in cell) from one crystal phase (the initial state, IS) to another (the final state, FS), which constitutes the reaction coordinates of the reaction, i.e., $Q_{\text{IS}}(L, q) \rightarrow Q_{\text{FS}}(L, q)$. In one SSW pathway sampling simulation, we need to collect as many as possible such IS/FS pairs (typically a few hundreds) to ensure the identification of the best reaction coordinate, the one corresponding to the lowest energy pathway. With such a pair of reaction coordinates, $Q_{\text{IS}}(L, q)$ and $Q_{\text{FS}}(L, q)$, it is then possible to utilize variable-cell double-ended surface walking (VC-DESW)²² method to identify the reaction transition state (TS) and the minimum energy pathway.

In our implementation, the SSW pathway sampling is fully automated and divided into three stages in simulation, namely, (i) pathway collection via extensive SSW global search; (ii) pathway screening via fast DESW pathway building;¹⁹ and (iii) lowest energy pathway determination via DESW TS search. The first stage is the most important and most time-consuming part, which generates all the likely pairs of generalized reaction coordinates linking different crystal phases. For example, for the olivine-spinel Mg_2SiO_4 phase transition in this work, we have collected more than 1000 pairs $Q_{\alpha}(L, q)$ and $Q_{\beta}(L, q)$, which leads to the finding of the lowest energy pathway. More details on the SSW pathway sampling are described in the [Supporting Information](#) and also in our previous works.¹⁹

All calculations, including the global exploration of the phase space of Mg_2SiO_4 crystal and the reaction sampling, were carried out in a supercell containing 28 atoms ($4\text{Mg}_2\text{SiO}_4$) at 15 GPa based on plane-wave density functional theory (DFT) calculations. The PES sampling was further checked using classical force fields²³ SSW search, showing no new low energy structures, where more than 10^6 minima are sampled and a larger supercell (56-atom) in simulation is utilized.

2.2. DFT Calculation Details. All calculations were performed using the plane wave DFT program, Vienna ab initio simulation package VASP,^{24,25} where electron–ion interaction was represented by the projector augmented wave (PAW)²⁶ pseudopotential and the exchange–correlation functional utilized was GGA-PBE.²⁷ In the pathway sampling, we adopt the following setups to speed up the PES exploration: plane-wave cutoff 400 eV; the Monkhorst–Pack k-point mesh of $(4 \times 4 \times 4)$ set for 28-atom supercell. The reference configurations for valence electrons were 2s2 2p4 for O, s2 for Mg, and s2p2 for Si. To obtain accurate energetics for the pathways, a more accurate calculation setup was utilized: the plane-wave cutoff 500 eV; the k-point mesh up to $(6 \times 4 \times 6)$ set and 8-electron (p6s2) PAW pseudopotential for Mg. For all the structures, both lattice and atomic positions were fully optimized until the maximal stress component is below 0.1 GPa and the maximal force component below 0.01 meV/Å, which leads to the convergence of the relative energy (e.g., barrier) below 0.5 meV/atom.

3. RESULTS AND DISCUSSION

Our investigation starts by exploring the phase space of Mg_2SiO_4 using first-principles SSW global structure search,^{17,18} which was carried out in a supercell containing 28 atoms ($4\text{Mg}_2\text{SiO}_4$) at 15 GPa based on plane-wave DFT calculations. More than 10^4 minima on the potential energy surface were visited from the SSW search, based on which we can provide an overview of Mg_2SiO_4 phase space. As shown in Figure 2, we

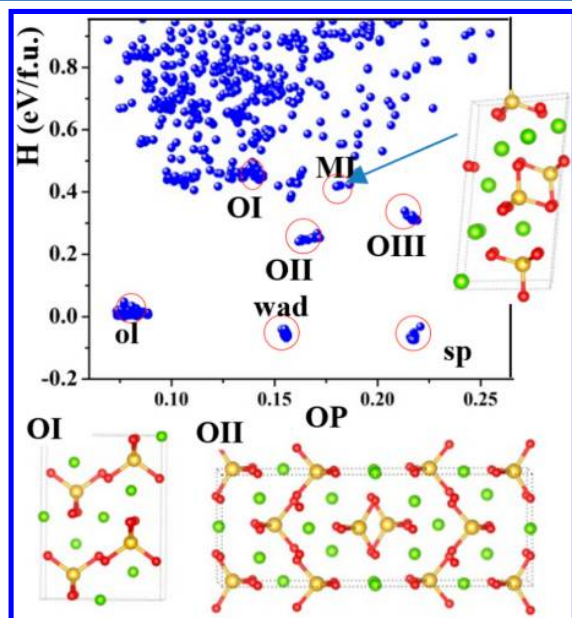


Figure 2. DFT enthalpy again order parameter (OP) for Mg_2SiO_4 phases obtained from SSW global structure search. The less stable OI, OII, and MI crystal structures are shown for their relevance in the reaction pathways. O atom: red ball; Mg atom: green ball; Si atom: yellow ball.

plot the DFT enthalpy H ($H = E + PV$) of optimized minima on potential energy surface against the structure order parameter. The order parameter utilized is a distance-weighted Steinhardt-type order parameter with angular moment $L = 2$,²⁸ which as a fingerprint for structure can distinguish different minima in the huge phase space. The important crystalline structures (phases) are indicated in the figure.

We found that only three low-lying crystalline phases are present within a 0.3 eV/f.u. (formula unit) window above olivine phase, i.e., olivine, wadsleyite, and spinel (0.1 eV/f.u. lower than olivine), which is consistent with the known thermodynamics that all these three phases are possible to present in nature at 15 GPa. Each crystalline phase is quite separated in the phase space as shown in the $H \sim OP$ plot. Geometrically, wadsleyite contains Si_2O_7 pairs with Si–O–Si–O linkage (double tetrahedra), while only lonesilicate oxoanion (SiO_4) units are present in olivine and spinel (Figure 1a).

The PES of Mg_2SiO_4 then enters into the amorphous-like region above 0.4 eV/f.u., where many energy degenerate conformations are present. The large gap between the stable crystalline structures and the amorphs region identified from Figure 2 implies that this silicate material has a high stability as the crystalline forms (e.g., high melting point). We will show later that indeed it requires a high kinetic barrier to transform from one crystal to another. For the less stable phases, we identify several high symmetry new phases, including orthorhombic OI (*Cmc*21, #63), OII (*Cmcm*, #36), and OIII (*Pbam*, #55) and monoclinic MI (*C2*, #5) (see Figure 2 structures and SI for detailed lattice data). All of them contain only lone SiO_4 tetrahedra in crystal, which are structurally close to olivine and spinel but differ from wadsleyite.

Our next task is to identify the lowest energy reaction pathway linking the olivine and spinel crystal phases. This is equivalent to build the fast connectivity between two known minima on multidimensional PES, a general challenge in the PES search. We utilized the recently developed SSW reaction sampling^{17,18} for crystal systems in this work, which has been

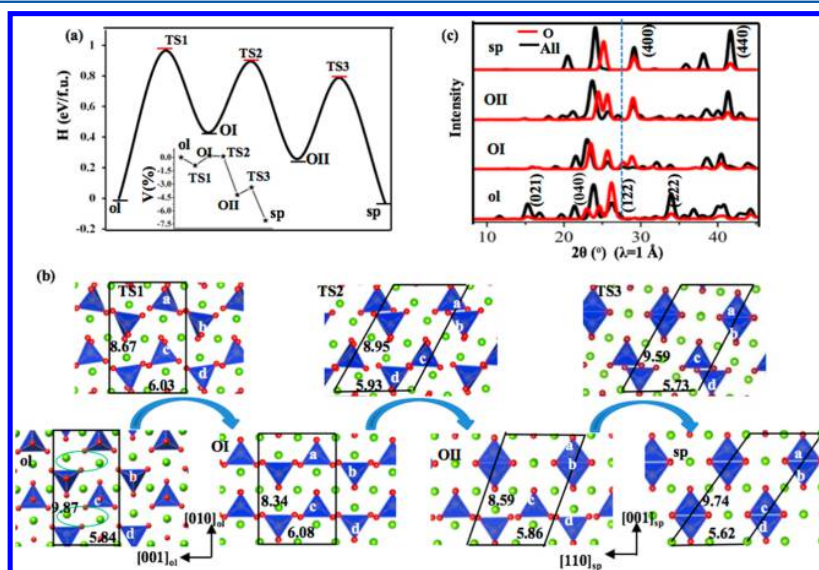


Figure 3. (a) Potential energy (enthalpy) profile for the lowest energy pathway for Mg_2SiO_4 olivine-spinel solid phase transition identified from SSW reaction sampling. The volume changes along the pathway are shown in the inset. (b) Reaction snapshots along the pathway. All structures are viewed along $[100]_{\text{ol}}$ or $[110]_{\text{sp}}$. The lattice is indicated by the black box with the lattice parameters being labeled in Å. O atom: red ball; Mg atom: green ball; Si atom: blue tetrahedron. (c) Simulated XRD patterns of the minima along the pathway.

successfully applied for single-element, binary metal and metal oxide systems. For the ternary Mg_2SiO_4 oxide encountered, we found that the PES is much more complex and therefore it challenges the current pathway sampling for finding the lowest energy pathway.

By sampling extensively both olivine and spinel crystal phases using SSW reaction sampling, we have collected more than 1000 pathways linking the two crystal phases, from which the lowest energy pathway is obtained by locating explicitly the TS of the reaction and sorting the computed barriers. The reaction enthalpy profile is plotted in Figure 3a, showing that the pathway is indirect, mediated by two high-energy OI and OII intermediate crystal phases (Figure 2). Interestingly, we note that wadsleyite does not act as an intermediate from olivine to spinel, confirming the previous suggestions from experiment.²⁹ The overall enthalpy barrier for the transition is high, 0.96 eV/f.u., dictated by TS1 of the first step, olivine to OI (The barrier drops to 0.70 eV/f.u. at 1500 K, see SI for free energy corrections via phonon calculations).

Figure 3b highlights the reaction snapshots of the solid transition viewed along $[100]_{\text{ol}}$. A salient feature for atomic motion is that all SiO_4 entities are maintained during the reaction without Si–O bond breaking. To further assist understanding the change of crystal structures, we also simulated XRD patterns for olivine, OI, OII and spinel phases, where both the overall pattern (black curve) and that originated from the O sublattice (red curve) are monitored and plotted in Figure 3c.

By inspecting the lattice variation, we can distinguish the first step from the other two steps. The first step, olivine-to-OI, has little overall volume change (1.8%) (Figure 3a, inset): a large lattice compression (+15.5%) occurs at $[010]_{\text{ol}}$ that is compensated by the expansion at $[001]_{\text{ol}}$ and $[100]_{\text{ol}}$. By contrast, the second and the third steps undergo large volume expansion (Figure 3a, inset) with appreciable lattice deformation due to the shearing of atoms on $(010)_{\text{ol}}$ along $[001]_{\text{ol}}$, a $(010)[001]_{\text{ol}}$ slip system. This leads to the variation of the lattice angle α from 90° to 54.7° on going from OI to spinel. Indeed, the unit cells of these shearing planes are similar, all being rectangular with close lattice length: $(010)_{\text{ol}}$: $4.69 \times 5.84 \text{ \AA}$; $(010)_{\text{OI}}$: $5.35 \times 6.08 \text{ \AA}$; $(010)_{\text{OII}}$: $5.48 \times 5.86 \text{ \AA}$; and $(010)_{\text{sp}}$: $5.62 \times 5.62 \text{ \AA}$. In the transition, $(100)_{\text{ol}}$ evolves into $(100)_{\text{OI}}$ and $(100)_{\text{OII}}$ and finally ends as $(1\bar{1}0)_{\text{sp}}$, where the close-packed O rows along $[001]_{\text{ol}}$ turns into that along $[110]_{\text{sp}}$, i.e. yielding an OR $(100)_{\text{ol}}/(1\bar{1}0)_{\text{sp}} + [001]_{\text{ol}}/[110]_{\text{sp}}$.

For the great similarity in the O sublattice of two phases, one may wonder naturally why the lowest energy pathway determined from theory does not involve the simple shearing of close-packing O layers (see Figure 1) but prefers the buckling of the close-packing O layer during the reaction. We found that this is mainly because the presence of strong Si–O bonds disallows the shearing of close-packing O layers that, if occurs, will break the Si–O bond and thus increase the energy cost of phase transition. Instead, the reaction adopts silicate oxoanion $[\text{SiO}_4]$ rigid-body rotation (olivine-to-OI) and translation (OI-to-spinel) without breaking Si–O bonds. On the other hand, the Mg cations change their coordination from six to four and back to six during the reaction, which contributes to the high barrier of the solid phase transition.

Specifically, from olivine to OI, SiO_4 tetrahedra move close at $[010]_{\text{ol}}$ which attenuates the $(122)_{\text{ol}}$ peak in XRD, but leads to the appearance of a $(020)_{\text{OI}}$ peak, both contributed mainly by

the O sublattice. The $(020)_{\text{OI}}$ peak eventually turns into $\{400\}_{\text{sp}}$. The atom movement in the first step is therefore dominated by the inner-rotation of SiO_4 tetrahedrons with the displacement of each O up to 1.4 Å, while Mg and Si cations stay largely in their original position (in fractional coordinate). Because of the rotation of SiO_4 , four Mg cations per supercell (circled in Figure 3b) change from octahedral to tetrahedral coordination. From OI to spinel, the two steps shear different layers of $(010)_{\text{ol}}$ along $[001]_{\text{ol}}$ (or $[110]_{\text{sp}}$), which leads to the pairing of SiO_4 tetrahedrons along $[001]_{\text{sp}}$ viewed along $[1\bar{1}0]_{\text{sp}}$ (Figure 3b). It is no wonder that the XRD patterns of OI, OII, and spinel phases are similar, especially for the (311) , (400) , and (440) peaks of spinel. The shearing is accompanied by volume compression, by 3.8% in OI-to-OII and 3.0% in OII-to-spinel. In these two steps, the tetrahedral Mg cations (circled in Figure 3b) have the largest atomic displacement, up to 2 Å per atom, which moves them from tetrahedral back to octahedral sites. These two steps resemble the shear-induced martensitic phase transition, and the computed phonon spectrum at the TS confirms the collective shearing mechanism (Figure S1 in SI).

Our results reveal that the characteristic $(400)_{\text{sp}}$ peak in XRD appears indeed early in the reaction, i.e. at the first intermediate OI phase. This confirms the observation by *in situ* XRD.^{15,16} Since $(400)_{\text{sp}}$ mainly originates from the O sublattice, it was inferred that the O fcc sublattice forms much earlier than cation sublattice. The cation motion was thus deduced to move excessively slower than O anion. However, from the lowest energy pathway, we find that this interpretation of *in situ* XRD data may not be correct. In fact, the SiO_4 tetrahedrons travel continuously together with Mg cations even at the final OII-to-spinel step. We conclude that the early appearance of $(400)_{\text{sp}}$ is a geometry reflection of the pathway: the condensation of olivine at $[010]_{\text{ol}}$ followed by $(010)_{\text{ol}}$ slip along $[001]_{\text{ol}}$.

With knowledge of the patterns of atomic displacement, it is interesting to ask whether a coherent interface is present during the solid phase transition. The coherent interfaces are generally present in martensitic solid phase transition systems, which can facilitate the new phase nucleus formation and propagation.³⁰ By using the numerical procedure to analyze the lowest energy pathway as developed previously based on phenomenological theory of martensitic crystallography,^{31,32} we fail to identify any coherent interface between olivine and spinel, which requires the perfect atomic match (overlap of two phases at the interface) and the lowest lattice strain.^{33,34} The best atomic match biphasic interface identified from this work is $(100)_{\text{ol}}/(1\bar{1}0)_{\text{sp}}$, as constructed in Figure 4a, which is 35 degrees off the putative $(100)_{\text{ol}}/\{111\}_{\text{sp}}$ interface in the literature (Figure 4b). These two orientations were recently observed in shocked meteorites by stereographic pole projections,³⁵ but we find that both of them do not meet the criteria for coherent interface.

The $(100)_{\text{ol}}/(111)_{\text{sp}}$ interface, although it has a low lattice misfit (0.7% strain along $[010]_{\text{ol}}$), has a large magnitude of atomic mismatch. On the other hand, the biphasic interface $(100)_{\text{ol}}/(1\bar{1}0)_{\text{sp}}$ determined from the lowest energy pathway has a better atomic match: SiO_4 and Mg of olivine only need to experience a local rotation and diffusion to reach to their positions in spinel. However, the $(100)_{\text{ol}}/(1\bar{1}0)_{\text{sp}}$ develops a large strain along $[010]_{\text{ol}}$ ($\sim 12.1\%$). This indicates that the nascent spinel nuclei inside the olivine matrix are unstable, inducing a large stress field, and thus the olivine-spinel transformation should be governed by incoherent nucleation and growth kinetics. The theoretical finding is consistent with

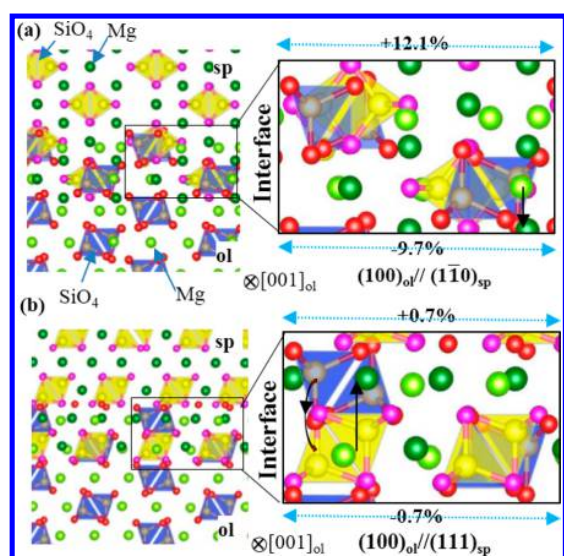


Figure 4. Heterophase junction models between olivine and spinel. (a) The $(100)_{\text{ol}}/(1\bar{1}0)_{\text{sp}}$ interface identified from the lowest energy solid phase transition pathway. The interface has close atomic match, but the lattice misfit is up to 12.1% along $[010]_{\text{ol}}$ (or $[001]_{\text{sp}}$). (b) The atomic model for the putative $(100)_{\text{ol}}/(111)_{\text{sp}}$ interface suggested from a martensitic model,⁶ where half of the atoms, SiO_4 and Mg, at the interface (enlarged on the right) are poorly matched atomically and the significant relocation is required for Si and Mg cations, as indicated by the black arrows. Both interfaces from (a) and (b) models are found to be incoherent.

the fact of the preferential spinel growth at the olivine grain-boundaries and dislocations.^{4,12,13}

The above results show that the origin of the high barrier in Mg_2SiO_4 phase transition is the change of bonding environment of Mg cation during the reaction. It is thus anticipated that the chemical composition would have a significant effect on the kinetics. Experimentally, the dramatic effect of chemical composition on the reaction kinetics has been observed. Increasing the iron content in olivine decreases the pressure of the phase transition. The pure magnesium end member, Mg_2SiO_4 (forsterite), transforms to ringwoodite at pressures above 14 GPa. At about 0.8 mole fraction fayalite (Fe_2SiO_4), olivine transforms directly to ringwoodite over the pressure range 10.0 to 11.5 GPa. Fayalite transforms to Fe_2SiO_4 spinel at pressures below 5 GPa.^{36–38}

To examine this effect from theory, we have investigated the role of cation species on the kinetics of olivine-to-spinel phase transition by focusing on the olivine to OI reaction step, the rate-determining step in olivine-to-spinel phase transition (In this step, the coordination for half of Mg cations reduce from six to four per supercell). We have considered to replace Mg with Fe or Zn, giving Fe_2SiO_4 , Zn_2SiO_4 . These elements are commonly present in the Earth's mantle and often mixed in olivine, such as $(\text{MgFe})_2\text{SiO}_4$. Using the lowest energy pathway shown in Figure 3, we have reoptimized the reaction pathway from olivine to OI at 15 GPa and determined the barrier using DFT calculations (For Fe_2SiO_4 , spin-polarized DFT+U calculations are utilized with the parameters of $U = 3.5$ eV for 3d orbital taken from the literature^{39,40}). All these A_2BO_4 oxides have stable minima geometry as olivine and OI phases, implying the similar PES features as Mg_2SiO_4 . As shown in Table 1, we found that the barrier can be dramatically reduced once Mg is replaced by Fe and Zn elements. For example, the

Table 1. Relative Enthalpies at 15 GPa from Olivine to OI Phase Transition and Key Structural Information by Replacing Mg by Fe or Zn Element^a

phase	states	H (eV/f.u.)	$d(\text{X}^{2+}\text{-O})$ (Å)	volume ($\text{\AA}^3/\text{f.u.}$)
Mg_2SiO_4	ol	0	2.04	67.64
	TS1	0.96	2.15	67.02
	OI	0.43	2.05	67.89
Fe_2SiO_4	ol	0	2.11	71.43
	TS1	0.47	2.06	70.34
	OI	0.12	2.10	70.47
Zn_2SiO_4	ol	0	2.09	69.93
	TS1	0.34	2.02	69.96
	OI	0.06	2.07	69.04

^a $d(\text{X}^{2+}\text{-O})$ is the average bond length for Mg–O, Fe–O, or Zn–O bonds.

barrier for Fe_2SiO_4 olivine–OI transition decreases to 0.47 eV/f.u., much smaller than the barrier for Mg_2SiO_4 0.96 eV/f.u. For Zn_2SiO_4 , the barrier is even lower than the barrier in Fe_2SiO_4 . This barrier decrease is obviously not due to the structural factors, as the bond distances of Mg–O, Fe–O, and Zn–O are very close. The computed data for kinetic order, $\text{Mg} > \text{Fe}$, is consistent with the observation in experiment.³⁶ It confirms that the bonding strength of the octahedral cation plays a critical role in A_2BO_4 oxide stability.

By analyzing the electronic structure for the key reaction step, we can better understand why the chemical composition is critical to the phase transition kinetics. As shown in Figure 5, we have plotted the total density of states (DOSs) for Mg_2SiO_4 (Figure 5a) and Fe_2SiO_4 (Figure 5c) at the TS1, and the projected DOS on the Mg (Figure 5b) and Fe (Figure 5d) cations of the system. As shown, we found that both oxides are insulating materials with a large band gap, where the valence bands (VB) mainly come from the O anion p states and the conduction bands (CB) are mainly constituted by cation states. Importantly, the lowest CBs in both systems are mainly from Mg or Fe cations, instead from Si cations, being the antibonding states of Mg–O or Fe–O bonds. This indicates that the Mg–O or Fe–O bonds belong to the weakest bonds in the system and are thus vulnerable for bond breaking during the solid phase transition. The Si–O bonds being the strong bonding in the ternary oxide prefer to be intact in the reaction to maximally reduce the energy cost. On the other hand, the replacement of Mg by Fe has reduced significantly the band gap, and introduce strong spin-splitting for the states at the top of VBs and the bottom of CBs. These states have strong features of 3d orbitals of Fe, which are not present in sp metal Mg, causing the substantial reduction of band gap in Fe_2SiO_4 . Because these 3d states of Fe are contracted with strong spin-polarization, their orbital mixing with p states of O anions is rather weak and contributes negatively in the octahedral bonding field. It is therefore much more facile for Fe to change its coordination environment, i.e., from octahedral to tetrahedral bonding, which helps to decrease the reaction barrier in the olivine-to-spinel solid phase transition.

4. CONCLUSIONS

This work by using the SSW potential energy surface sampling method reveals a new mechanism for a ternary silicate crystal-to-crystal solid phase transition, Mg_2SiO_4 olivine to spinel transition, which represents a common transition in A_2BO_4 oxides. We show that the phase transition of this inorganic

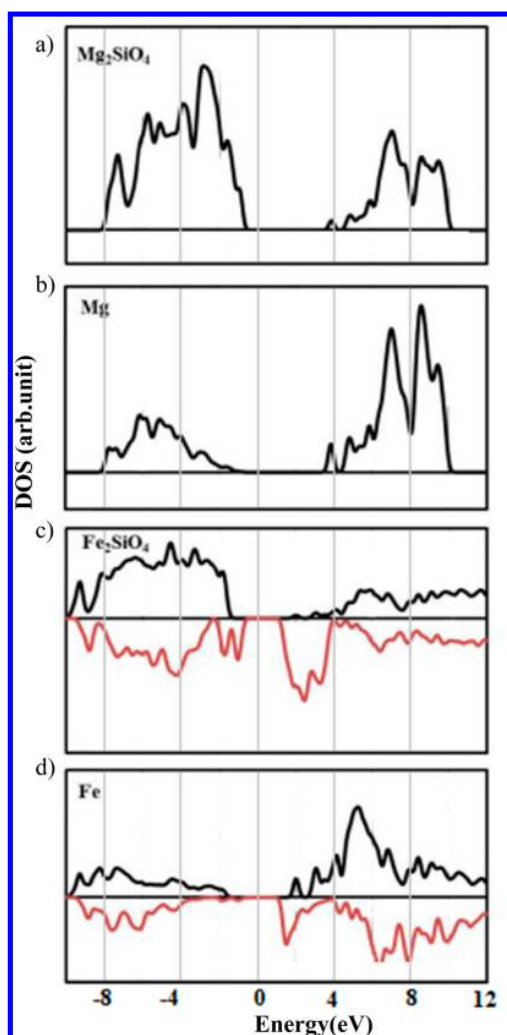


Figure 5. Density of states (DOS) and the projected DOS at the TS1 for Mg_2SiO_4 and Fe_2SiO_4 . (a and c) Total DOSs of the two systems; (b and d) projected DOSs onto Mg and Fe cations of the two systems. For Fe_2SiO_4 system, the majority spin and the minority spin are plotted with black and red colors, respectively.

mineral system behaves unexpectedly like molecular crystal systems, where silicate oxoanion SiO_4 tetrahedron moves as a molecular entity during the pressure-induced solid phase transformation. The high barrier of Mg_2SiO_4 solid transition, or alternatively speaking, the high stability of Mg_2SiO_4 , is attributed to the strong ionic bonding between Mg^{2+} and O^{2-} that prefers octahedron coordination. The replacement of Mg by Fe and Zn cations can significantly reduce the phase transition barrier and thus introduce instability in the cation-doped materials. We believe that the PES sampling method utilized here is of general applications for revealing complex solid phase transition kinetics, which can guide the design of stable materials with desirable mechanical and electronic properties.

■ ASSOCIATED CONTENT

Supporting Information

This information is available from The Supporting Information is available free of charge on the ACS Publications website at DOI: 10.1021/acs.jpcc.6b08942.

More details on calculation methods; lattice parameters for crystalline phases; phonon spectrum of key states; pressure and temperature effects on the reaction barriers; atomic XYZ positions for all the states along the pathway. (PDF)

■ AUTHOR INFORMATION

Corresponding Author

*E-mail: zpliu@fudan.edu.cn.

Notes

The authors declare no competing financial interest.

■ ACKNOWLEDGMENTS

This work is supported by National Science Foundation of China (21533001), Science and Technology Commission of Shanghai Municipality (08DZ2270500).

■ REFERENCES

- (1) Wentzcovitch, R. M.; Yu, Y. G.; Wu, Z. Thermodynamic Properties and Phase Relations in Mantle Minerals Investigated by First Principles Quasiharmonic Theory. *Rev. Mineral. Geochem.* **2010**, *71* (1), 59–98.
- (2) Deuss, A.; Woodhouse, J. Seismic observations of splitting of the mid-transition zone discontinuity in Earth's Mantle. *Science* **2001**, *294*, 354–357.
- (3) Wu, T. C.; Bassett, W. A.; Burnley, P. C.; Weathers, M. S. Shear-promoted phase transitions in Fe_2SiO_4 and Mg_2SiO_4 and the mechanism of deep earthquakes. *J. Geophys. Res.* **1993**, *98* (B11), 19767–19776.
- (4) Kirby, S. H.; Stein, S.; Okal, E. A.; Rubie, D. C. Metastable mantle phase transformations and deep earthquake in subducting oceanic lithosphere. *Rev. Geophys.* **1996**, *34*, 261–306.
- (5) Sung, C. M.; Burns, R. G. Kinetics of the olivine to spinel transitions to deep-focus earthquake genesis. *Earth Planet. Sci. Lett.* **1976**, *32*, 165–170.
- (6) Poirier, J. P. Martensitic olivine-spinel transformation and plasticity of the mantle transition zone. *Anelasticity in the Earth. Geodynamics Series*; American Geophysical Union: Washington, DC, **1981**; Vol. 4, pp 113–117.
- (7) Lacam, A.; Madon, M.; Poirier, J. P. Olivine glass and spinel formed in a laser heated, diamond-anvil high pressure cell. *Nature* **1980**, *288*, 155–157.
- (8) Green, H. W.; Burnley, P. C. A new self-organizing mechanism for deep-focus earthquakes. *Nature* **1989**, *341* (26), 733–737.
- (9) Madon, M.; Guyot, F.; Peyronneau, J.; Poirier, J. P. Electron microscopy of high-pressure phases synthesized from natural olivine in diamond anvil cell. *Phys. Chem. Miner.* **1989**, *16*, 320–330.
- (10) Boland, J. N.; Liu, L. G. Olivine to spinel transformations in Mg_2SiO_4 via faulted structures. *Nature* **1983**, *19*, 233–235.
- (11) Burnley, P. C.; Green, H. W. Stress dependence of the mechanism of the olivine-spinel transformation. *Nature* **1989**, *338*, 753–756.
- (12) Brearley, A. J.; Rubie, D. C.; Ito, E. Mechanisms of the transformation between the α , β and γ polymorphs of Mg_2SiO_4 at 15 GPa. *Phys. Chem. Miner.* **1992**, *18*, 343–358.
- (13) Kerschhofer, L.; Rubie, D. C.; Sharp, T. G.; McConnell, J. D. C.; Dupas-Bruzek, C. Kinetics of intracrystalline olivine-ringwoodite transformation. *Phys. Earth Planet. Inter.* **2000**, *121*, 59–76.
- (14) Vaughan, P. J.; Green, H. W.; Coe, R. S. IS the olivine-spinel transformation martensitic? *Nature* **1982**, *298*, 357–358.
- (15) Furnish, M. D.; Bassett, W. A. Investigation of the mechanism of the olivine-spinel transition in fayalite by synchrotron radiation. *J. Geophys. Res.* **1983**, *88* (B12), 10333–10341.
- (16) Chen, J.; Weidner, D. J.; Parise, J. B.; Vaughan, M. T.; Raterron, P. Observation of cation reordering during the olivine-spinel transition

in fayalite by in situ synchrotron X-ray diffraction at high pressure and temperature. *Phys. Rev. Lett.* **2001**, *86* (18), 4072–4075.

(17) Shang, C.; Liu, Z. P. Stochastic Surface Walking Method for Structure Prediction and Pathway Searching. *J. Chem. Theory Comput.* **2013**, *9* (3), 1838–1845.

(18) Zhang, X. J.; Shang, C.; Liu, Z. P. From Atoms to Fullerene: Stochastic Surface Walking Solution for Automated Structure Prediction of Complex Material. *J. Chem. Theory Comput.* **2013**, *9* (7), 3252–3260.

(19) Zhang, X. J.; Shang, C.; Liu, Z. P. Double-Ended Surface Walking Method for Pathway Building and Transition State Location of Complex Reactions. *J. Chem. Theory Comput.* **2013**, *9* (12), 5745–5753.

(20) Zhang, X. J.; Liu, Z. P. Reaction Sampling and Reactivity Prediction Using Stochastic Surface Walking Method. *Phys. Chem. Chem. Phys.* **2015**, *17*, 2757–2769.

(21) Shang, C.; Zhang, X. J.; Liu, Z. P. Reaction Sampling and Reactivity Prediction Using Stochastic Surface Walking Method. *Phys. Chem. Chem. Phys.* **2014**, *14*, 17845–17856.

(22) Zhang, X. J.; Liu, Z. P. Variable-cell double-ended surface walking method for fast transition state location of solid phase transitions. *J. Chem. Theory Comput.* **2015**, *11* (10), 4885–4894.

(23) Matsui, M. Computational modeling of crystals and liquids in the system $\text{Na}_2\text{O-CaO-MgO-Al}_2\text{O}_3\text{-SiO}_2$. *Geoph. Monog.* **1998**, *101*, 145–151.

(24) Kresse, G.; Furthmüller, J. Efficient iterative schemes for ab initio total-energy calculations using a plane-wave basis set. *Phys. Rev. B: Condens. Matter Mater. Phys.* **1996**, *54* (16), 11169–11186.

(25) Kresse, G.; Furthmüller, J. Efficiency of ab-initio total energy calculations for metals and semiconductors using a planewave basis set. *Comput. Mater. Sci.* **1996**, *6*, 15–50.

(26) Blöchl, P. E. Projector augmented-wave method. *Phys. Rev. B: Condens. Matter Mater. Phys.* **1994**, *50* (24), 17953–17979.

(27) Perdew, J. P.; Burke, K.; Ernzerhof, M. Perdew, Generalized gradient approximation made simple. *Phys. Rev. Lett.* **1996**, *77* (18), 3865.

(28) Steinhardt, P. J.; Nelson, D. R.; Ronchetti, M. Bond-orientational order in liquids and glasses. *Phys. Rev. B: Condens. Matter Mater. Phys.* **1983**, *28* (2), 784–805.

(29) Perrillat, J. P.; Daniel, I.; Bolfan-Casanova, N.; Chollet, M.; Morard, G.; Mezouar, M. Mechanism and kinetics of the α - β transition in San Carlos olivine $\text{Mg}_{1.8}\text{Fe}_{0.2}\text{SiO}_4$. *J. Geophys. Res. Solid Earth* **2013**, *118* (1), 110–119.

(30) Guan, S. H.; Liu, Z.-P. Anisotropic Kinetics of Solid Phase Transition from First Principles: Alpha-Omega Phase Transformation of Zr. *Phys. Chem. Chem. Phys.* **2016**, *18*, 4527–4534.

(31) Bowles, J. S.; Mackenzie, J. K. The crystallography of martensite transformations I. *Acta Metall.* **1954**, *2*, 129–137.

(32) Laudau, L. D.; Lifshitz, E. M. *Statistical Physics*; Addison Wesley: Salt Lake City, UT, 1958.

(33) Zhao, W. N.; Zhu, S. C.; Li, Y. F.; Liu, Z. P. Three-phase Junction for Modulating Electron-Hole Migration in Anatase/Rutile Photocatalysts. *Chem. Sci.* **2015**, *6* (6), 3483–3494.

(34) Guan, S. H.; Zhang, X. J.; Liu, Z. P. Energy Landscape of Zirconia Phase Transitions. *J. Am. Chem. Soc.* **2015**, *137*, 8010–8013.

(35) Greshake, A.; Fritz, J.; Böttger, U.; Goran, D. Shear-induced ringwoodite formation in the Martian shergottite Dar al Gani 670. *Earth Planet. Sci. Lett.* **2013**, *375*, 383–394.

(36) Furnish, M. D.; Bassett, W. A. Investigation of the mechanism of the olivine-spinel transition in fayalite by synchrotron radiation. *J. Geophys. Res. Solid Earth* **1983**, *88* (B12), 10333–10341.

(37) Yagi, T.; Akaogi, M.; Shimomura, O.; Suzuki, T.; Akimoto, S. I. In situ observation of the olivine-spinel phase transformation in Fe_2SiO_4 using synchrotron radiation. *J. Geophys. Res.* **1987**, *92* (B7), 6207–6213.

(38) Frost, D. J. The structure and sharpness of $(\text{Mg,Fe})_2\text{SiO}_4$ phase transformations in the transition zone. *Earth Planet. Sci. Lett.* **2003**, *216* (3), 313–328.

(39) Mosey, N. J.; Liao, P.; Carter, E. A. Rotationally-Invariant ab initio Evaluation of Exchange and Coulomb Parameters for DFT+U Calculations. *J. Chem. Phys.* **2008**, *129*, 014103–014115.

(40) Li, Y. F.; Liu, Z. P. Structure and Water Oxidation Activity of 3d Metal Oxides. *WIREs Comput. Mol. Sci.* **2016**, *6*, 47–64.